25th ABCM International Congress of Mechanical Engineering
October 20-25, 2019, Uberlândia, MG, Brazil

COB-2019-0551
EXPERIMENTAL CHARACTERIZATION OF MODE I INTERLAMINAR FRACTURE TOUGHNESS IN LOW-MELT PAEK THERMOPLASTIC COMPOSITE MATERIAL

Natália R. Marinho, Mariano A. Arbelo, Francis Gonzalez, Geraldo M. Candido, Rita C. M. Sales, Mauricio V. Donadon
Aeronautics Division, Instituto Tecnológico de Aeronáutica-ITA, Praça Mal. Eduardo Gomes, 50, 12228-900, São José dos Campos-SP, Brazil
nmarinho@ita.br, marbelo@ita.br, francismgonzalezr@gmail.com, geraldomcan@gmail.com, rita.sales@fatec.sp.gov.br, donadon@ita.br

Abstract. *Mode I fracture is one of the most widely studied fracture modes in fiber-reinforced polymer structural composites research. On the other hand, fracture properties of thermoplastic structural composites have not been studied extensively. This paper presents the determination of opening Mode I strain energy release rate (G_I) for a reinforced thermoplastic laminate made by a semipreg plain-5H satin weave fabric and a semi-crystalline engineered polyarlyetherketone (PAEK) resin. Interlaminar fracture toughness was calculated based on Modified Beam Theory (MBT) method considering a perfectly built-in double cantilever beam. Experimental procedure and calculations to characterize Mode I interlaminar fracture toughness was performed according to Double Cantilever Beam (DCB) test method described in ASTM D5528-13 using end blocks to introduce opening forces. Comparisons with analytical solution using simple beam theory analysis was carried out to verify the obtained results. Finally, a fractography analysis was carried out in the tested samples to determine the failure mechanisms involved during the fracture process. Results demonstrated that thermoplastic composites usually present enhanced fracture toughness compared to thermosets. This improved fracture behavior is justified mainly due to the higher fracture resistance of crystalline polymers in comparison to amorphous polymers.*

Keywords: *Carbon fiber composites, Fracture mechanics, Thermoplastics, Mode I delamination*

1. INTRODUCTION

In recent years, there has been a clear demand for studies in new advanced composite materials for structural applications, such as new types of resin composition and fabric arrangements in order to optimize fracture properties. Within this context, investigations focused on the fracture behavior and properties of thermoplastic laminates are of utmost relevance. Thermoplastic polymer-based composites usually demand simpler fabrication cycles considering prepregs. Furthermore, these materials are more adequate to high-volume production than thermoset laminates mainly because no chemical reaction is needed. Besides the manufacturing process advantages, thermoplastic composites also demonstrate better fracture toughness, impact strength and chemical resistance than thermoset-based composites (Muzzy and Kays, 1988). Delamination is one of the most common failure mechanisms in composite laminates (O'Brien, 1998). Mode I delamination is induced by through-the-thickness interlaminar tensile normal stresses, which causes layer debonding in the direction normal to the interface. In this context, the experimental determination of Mode I critical strain energy release rate (G_{IC}) for TenCate Cetex® low-melt PAEK CT1225 fabric is presented and discussed in this paper. The proposed material features special characteristics over other composites with a PAEK family matrix like: reduction in processing temperature by 50 – 75 °C. This enables TenCate Cetex® TC1225 to be processed on machines with a lower temperature range, potentially reducing investment costs in both machines and tooling.

The results presented on this paper are related to the SPIRIT (São Paulo Initiative on Research into Thermoplastic Composites) initiative, proposed with the objective of establishing a local network for collaborative research on thermoplastics composites materials.

2. MODIFIED BEAM THEORY (MBT) METHOD

Mode I interlaminar fracture toughness is computed using MBT method, compliance calibration (CC) method or modified compliance calibration (MCC) method (American Society for Testing and Materials, 2013). All data reduction methods are adequate for measuring strain energy release rate G_I, but MBT is the recommended method because it returns the most conservative values (Murri, 2013).

The expression to compute the mode I interlaminar fracture toughness (G_I) based on the MBT is given by Eq.(1) (American Society for Testing and Materials 2013).

$$G_I = \frac{3P\delta}{2ba} \tag{1}$$

Where P = load, δ = load point displacement, b = specimen width and *a* = delamination length

Since the test specimen is not a perfectly clamped beam, this expression overestimates the strain energy release rate. In other words, a small rotation occurs at the tip of the delamination. To take in account this rotation effect, an additional parameter Δ needs to be added to the delamination length. The value of Δ may be determined experimentally through least squares plot of the cube root of compliance $C^{1/3}$ as a function of delamination length, as shown in Fig. 1 (American Society for Testing and Materials, 2013).

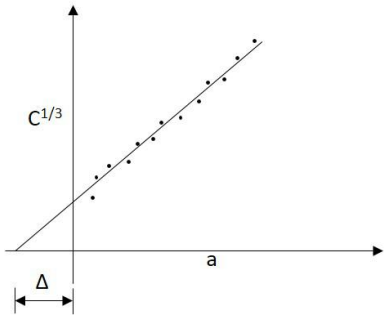

Figure 1. Δ calculation for MBT. Adapted from American Society for Testing and Materials (2013).

For the MBT Method, correlation between compliance *C* and crack length *a* has been shown to be given by (Murri 2013):

$$C^{1/3} = m(a + |\Delta|) \tag{2}$$

Additionally, large deflection corrections may be included in calculations of the strain energy release rate (American Society for Testing and Materials, 2013). Large displacement effects must be adjusted by the addition of a parameter F in the data reduction.

$$F = 1 - \frac{3}{10}\left(\frac{\delta}{a}\right)^2 - \frac{3}{2}\left(\frac{\delta t}{a^2}\right) \tag{3}$$

Where t is shown in Fig. 2.

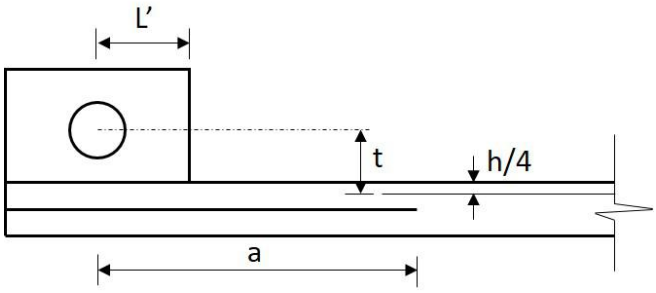

Figure 2 Illustration of geometrical parameters employed in the data reduction for DCB Specimen.

In order to consider the geometrically nonlinear effects induced by adding the loading blocks, a second parameter N must be added as a displacement correction

$$N = 1 - \left(\frac{L'}{a}\right)^3 - \frac{9}{8}\left[1 - \left(\frac{L'}{a}\right)^2\right]\left(\frac{\delta t}{a^2}\right) - \frac{9}{35}\left(\frac{\delta}{a}\right)^2 \tag{4}$$

Where L' and t are shown in Fig. 2.

Finally, the corrected fracture toughness is calculated as follows

$$G_I = \frac{F}{N}\frac{3P\delta}{2b\left(a + |\Delta|\right)} \tag{5}$$

3. THEORETICAL MODEL FOR DCB SPECIMEN

Simple beam theory analysis is use to verify the experimental data reduction. For DCB specimens in pure Mode I tests, the energy release rate G was deduced by Williams (1989) employing beam theory due to a delamination process, as illustrated in Fig. 3(a).

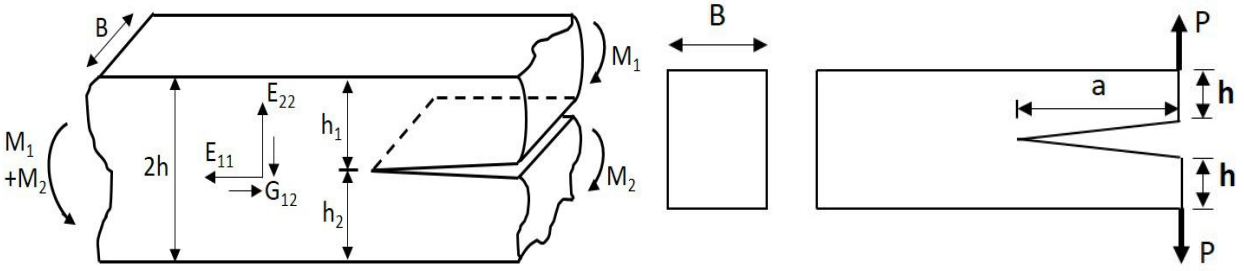

(a) Mode I under general bending

(b) Delamination of double cantilever beam specimen under mode I opening load

Figure 3. Composite laminate with crack under bending load. Adapted from Williams (1989)

Williams (1989) supposed a crack in a beam with a moment M_1 and M_2 applied on the upper and lower arm, respectively. The uncracked side is subjected to the sum of the moments ($M_1 + M_2$). Supposing a general bending, the change of potential energy with an increment in crack area, defined as the strain energy release rate, is described as follows (Williams, 1989):

$$G_I = \frac{3}{4B^2hE_{11}}\left\{\left(\frac{2h}{h_1}\right)^3 M_1^2 + \left(\frac{2h}{h_2}\right)^3 M_2^2 - \left(M_1 + M_2\right)^2\right\} \tag{6}$$

Where M_1 and M_2 are general loadings; B, h, h_1 and h_2 are defined in Fig. 3(a) and E_{11} is the specimen longitudinal modulus in the direction indicated in Fig. 3(a)

Considering pure opening mode for the standard DCB specimen (with an edge crack), the loading case gives $M_2 = -M_1 = Pa$, as shown for example in Fig. 3(b). Consequently, the crack extension force from Eq.(7) is

$$G_I = \frac{12P^2a^2}{B^2h^3E_{11}} \tag{7}$$

However, the equation based on simple beam theory requires corrections to take into account many effects, which are not predicted for this method (Kinloch, et al., 1993) . For instance, this solution neglects shear and bending deformations that occur at the tip of the delamination to estimate the strain energy release rate. A correction parameter

is added to the delamination length to account for these deformations effects, as presented in Eq.(8), Eq.(9) and Eq.(10) (Reeder, 2003).

$$G_I = \frac{12P^2(a+\chi h)^2}{B^2h^3E_{11}} \tag{8}$$

$$C = \frac{\delta}{P} = \frac{8(a+\chi h)^3}{Bh^3E_{11}} \tag{9}$$

Where the correction parameter is $\chi = \sqrt{\frac{E_{11}}{11G_{12}}\left\{3-2\left(\frac{\Gamma}{1+\Gamma}\right)^2\right\}}$ with $\Gamma = 1.18\frac{\sqrt{E_{11}E_{22}}}{G_{12}}$ (10)

Disregarding deformation effects from Eq.(9), the opening displacement at linear loading phase (δ_L) was predicted as given in Eq.(11), where average initial crack length value (a_0) and load vector (P) were used as input. The load vector (P) was defined in accordance with the minimum and maximum load at linear phase, that is from 0 to 240N every 30N.

$$\delta_L = \frac{8a_0^3P}{Bh^3E_{11}} \tag{11}$$

From Eq.(8), loading at propagation phase (P_P) was described as follows

$$P_P = \left(\frac{G_IB^2h^3E_{11}}{12a^2}\right)^{1/2} \tag{12}$$

Where G_I is the measured average energy release rate and a is crack length values from initial crack length to maximum observed crack length

Opening displacements at propagation phase (δ_P) were calculated as shown in Eq. (13).

$$\delta_P = \frac{8(a+\chi h)^3P_P}{Bh^3E_{11}} \tag{13}$$

The elastic mechanical properties needed for the analytical verification were measured using ASTM Standard D3039 and D3518 and the results are presented on Tab. 1.

Table 1. Elastic mechanical properties of TenCate Cetex® low-melt PAEK CT1225 fabric

E_{11} = E_{22} [GPa]	55.549
G_{12} [GPa]	3.773
ν_{12}	0.052

4. METHODOLOGY AND EXPERIMENTAL PROCEDURE

Quasi-static tests of Mode I transverse tensile were carried out on six specimens made out of low-melt PAEK Fabric, TC1225, 5HS, 280 g/m², T300J, 3K to obtain the fracture toughness and delamination resistance curves. The specimen's layup is $[(0, 90)]_{9s}$ and the average values of the measured width (b_{avg}), thickness (t_{avg}) and initial crack (a_0) are shown in Tab. 2.

The experimental procedure was carried out recommendations provided by ASTM Standard D5528 (American Society for Testing and Materials, 2013). The test consists in loading the specimen according to the setup depicted in Fig. 4. Delamination tests were performed under displacement control in a rate of 1mm/min.

Table 2. Test specimen geometry.

ID	t_{avg}	b_{avg}	a_0
	[mm]	[mm]	[mm]
1	5,64	20,08	40,19
2	5,69	20,09	35,95
3	5,64	20,10	38,07
4	5,66	20,11	39,12
5	5,74	20,08	44,41
6	5,73	20,07	45,47

Crack length was visually monitored and recorded together with the corresponding load and displacement at each crack propagation. Figure 5 shows an example of load vs displacement plot, including crack markers related to observed delamination lengths.

Figure 4. Experimental test setup of loading in Mode I

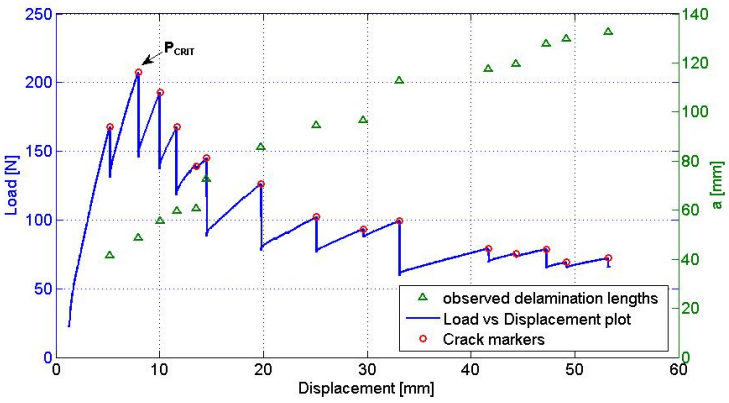

Figure 5. Example of load and crack opening vs displacement plot

For fractography analyses, 40mm samples width were cut at regions where the fracture process occurred. A vacuum pump QUORUM - Q150RE5 was used for coating the fracture surfaces with a thin gold film by sputtering process. The fracture morphology was analyzed using a scanning electron microscope (SEM) VEGA3 XMU TESCAN. Images of the characteristics fracture features were acquired using SE analyses with an acceleration voltage of 10kV, beam intensity of 10, a working distance of 20 mm and a magnification range from 55X to 10KX.

5. RESULTS

For all six specimens, critical fracture toughness was computed employing MBT Method. Least squares linear fit was use on the plot of the crack length a vs. the cube root of compliance $C^{1/3}$ to determine compliance parameters, the correction Δ and the slope m. Figure 6 shows the results of all the DCB specimens. A crack increment leads to a change in compliance which cause a loss of strain energy (Pagano, 1989). According to Eq.(2), using the results from all DCB specimens, the relationship between the compliance and delamination length was defined as $C^{1/3}=0.0062(a + |2.0351|)$ with Coefficient of Determination (R^2) equal to 0.9475, which indicates a good adjustment to a linear plot.

Delamination resistance curves are frequently applied to a comparative analysis of fiber-matrix interface between laminates (Murri, 2013). Weak fiber-matrix interface bonding generally results in a higher degree of fiber bridging and so a higher values of energy release rate with crack length (US Army Research Laboratory, 1999).

For laminates not greatly affected by fiber bridging, a pronounced stick-slip behavior is observed in the load-displacement curves. A stick-slip behavior is observed in Fig. 5 and it is related to the unstable crack growth followed

by a loss of applied load. Because of this behavior, greater toughness values were observed compared to subsequent crack grow (US Army Research Laboratory, 1999).

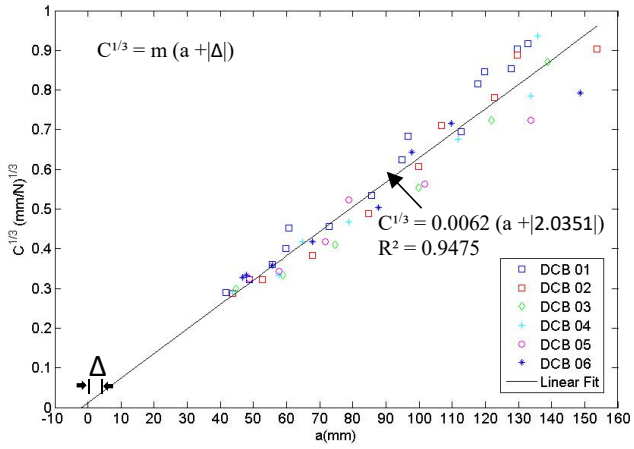

Figure 6. Linear fit to a *vs* $C^{1/3}$

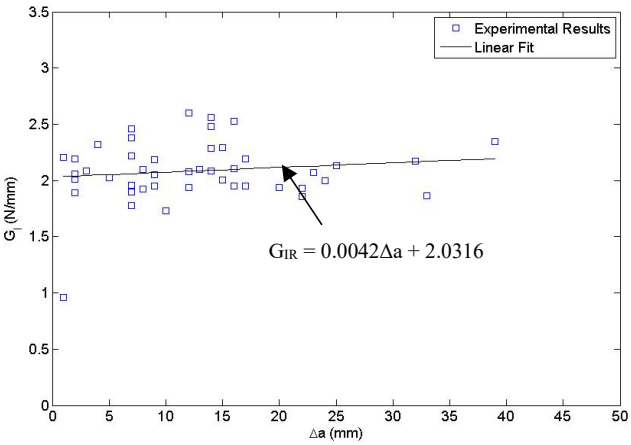

Figure 7. R-curve from DCB tests

The computed energies release rate G_I values were plotted vs. the associated crack grow (Δa) on the delamination resistance curve shown in Fig. 7. Considering a linear fit for R-curve, the equation that describes energy release rate in terms of crack increment is $G_{IR} = 0.0042\Delta a + 2.0316$. Despite the dispersion in values is reasonably large, the resistance curve for the tested specimens might be defined as flat, which can be confirmed by quite low angular coefficient provided by the linear fitting equation. According to the formulation exposed in section 2, the critical average fracture toughness obtained for each sample and its correspondent standard deviation are presented in Fig. 8.

Average energy release rate, considering all specimens, is equal to $G_{IRAVERAGE} = 2.08$ N/mm and its correspondent standard deviation is 0.2696. It is interest to notice that thermoplastic resin system exhibit a higher fracture toughness compared to thermoset ones. For instance, similar tests were performed using 0º carbon-epoxy prepregs fabric plies and the critical fracture toughness was found to be 3.5 times lower ($G_{IR\ THERMOSET} = 0.587$ N/mm) than the one presented on this paper (Toyoda, 2009).

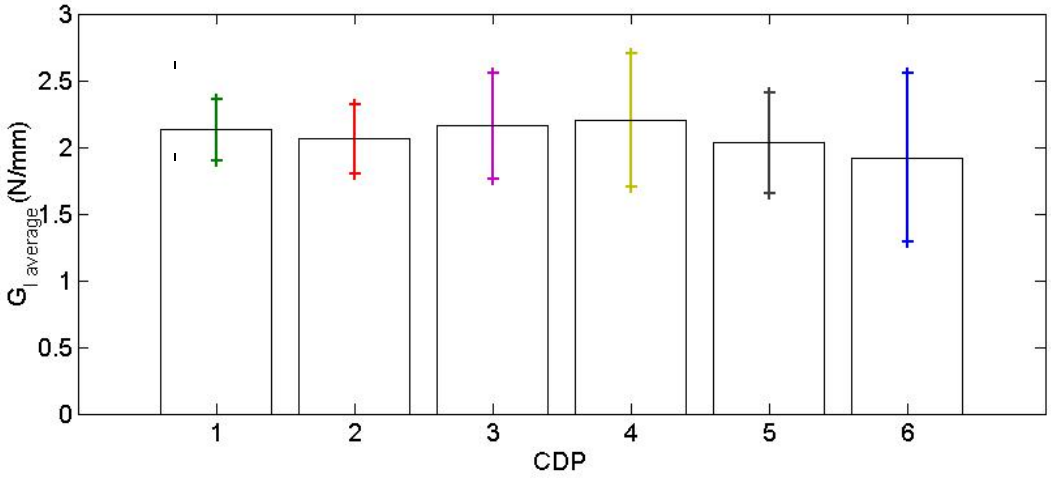

Figure 8. Average Mode I critical fracture toughness values for each DCB specimens with standard deviation

The experimental and analytical load vs. displacement curves are compared in Fig. 9. It is important to emphasize the very good correlation between experimental results and predictions obtained using the analytical model, where $G_{IRAVERAGE}$ was used as input. Woven laminates usually exhibit unstable crack growth (stick-slip effect) (Sacchetti, et al., 2017). The stick-slip behavior is a result of local increase of toughness (Hine, et al., 1989). Some authors have reported an overestimation on Mode I fracture toughness values which is related to the stick-slip behavior observed in the load-displacement curves (Sacchetti, et al., 2017).

Crack propagation speed decreases when the crack front get through these tougher domains until there is enough stored elastic energy to generate new crack surfaces. After the tougher region, the crack growth rate increases caused by

a higher elastic energy stored compared to the energy necessary for stable propagation (Sacchetti, et al., 2017). Tougher areas in woven composites are related to the regions where the crack go through weft cables (Ogasawara, et al., 2012).

From the plot of load vs. displacement, it can be noticed a linear behavior at the beginning of the test procedure until reaches the critical load and so the crack suddenly starts the propagation, followed by a decrease in load. This behavior is recurring and repeats throughout the test with a linear loading phase, succeeded by an abrupt decrease in load as the crack length increases. The linear loading phase provides the possibility of applying the linear elastic fracture mechanics (Sacchetti, et al. ,2017).

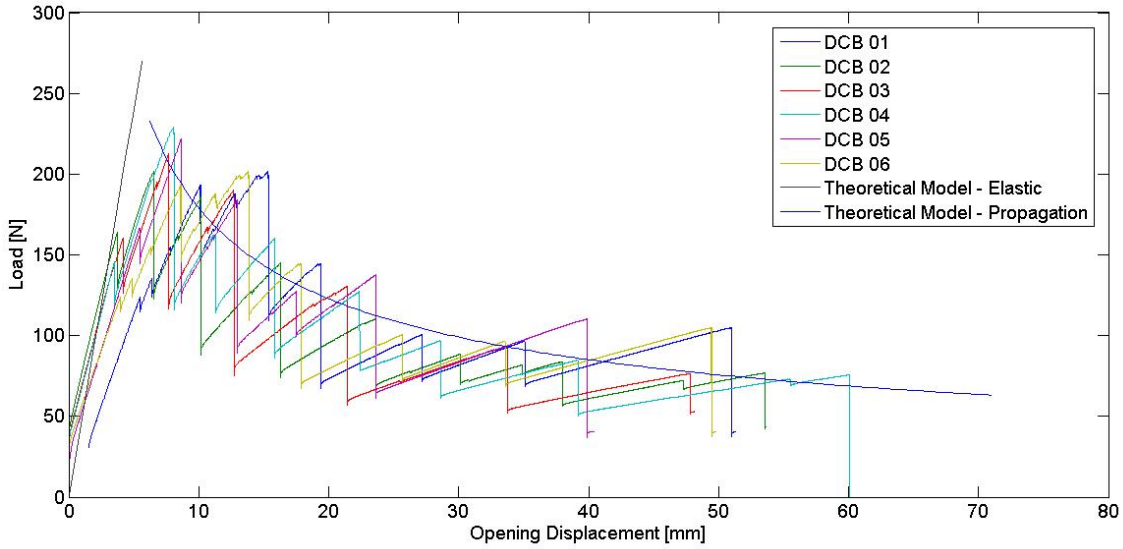

Figure 9. Load vs Opening Displacement plot

6. FRACTOGRAPHIC ANALYSIS

Accurate analysis of the fracture surface by use of microscopy technique contributes to an appropriate interpretation of data collected from the quasi-static delamination test. *Figure 10* shows images with different magnitudes of the fracture surfaces and significant interlaminar failure features of tested DCB specimens. In each image, the propagation direction of delamination (PD) occurs from left to right. In regards to 2D woven composites , the crack has a tendency to jump and advances following layers interfaces out of the mid-plane, developing non-self-similar crack growth and mixed-mode behavior (Pagano, 1989).

Mode I fracture toughness is affected by a non-uniform and irregular crack front and the observed tortuous of the crack path providing higher toughness values (Sacchetti, et al., 2017). For fabric laminates, crack propagation through matrix-rich regions and irregular tortuous crack path can be partially responsible for an increase in interlaminar toughness compared to unidirectional composites (Sacchetti, et al., 2017).

The presence of fast brittle fracture defined by scarps (Fig. 10.b.F), cusps (Fig. 10.a.C), feathering (Fig. 10.b.E) and riverlines (Fig. 10.b.G) are predominant and significant at the failure surface (Purslow, 1987). In the fast brittle interlaminar fracture of fiber-reinforced PAEK laminates, as with thermoset composites, feathering and riverlines features indicate the local crack propagation directions (Purslow, 1987).

Figure 10.a.A shows tidemarks that indicates stages of crack propagation and micro damage of the composite during the experiment. Tide marks are a common aspect in thermoplastics laminates and usually these microcracks refer to an alteration in crack grow rate or a momentary crack front arrest (Greenhalgh, 2009). These changes in crack velocity are related to a variation in the failure mechanism leading to an alteration in energy absorption (Purslow, 1987).

At slow crack speeds, ductility and large amount of plastic deformation of the matrix were observed close to interstitial site between warp/weft tows and it is related to unstable propagation. Highly matrix ductility and elevated composite delamination toughness results in large-scale plastic deformation as illustrated in Fig. 10.a.D. Fibers totally impregnated by the matrix in Fig. 10.d and Fig. 10.a suggests that ductile thermoplastic resin system demonstrate good fiber-matrix bonding (Greenhalgh, 2009). Figure 10.a.B and Figure 10.b.B exhibit broken fibers in warp direction which confirms strong fiber-matrix bonding. This feature is one of the reasons why thermoplastic composites exhibits higher fracture toughness compared to brittle thermoset resin (Muzzy and Kays, 1988). However, in slow-ductile failure, some fibers are not impregnated because of greater deformation of the matrix (see Fig. 10.c.I) (Purslow, 1987).

Mode I tension fracture surface of thermoplastic laminates exposes small matrix peaks as shown in Fig. 10.c.K at fiber tracks (Fig. 10.c.H). Purslow (1987) called ‘crazing’ to this slow ductile fracture in thermoplastic system, also known as fibrillation. The gross plasticity in the central region between two fiber cables defines a toughening

mechanism that will causes fibrillation at this area (Greenhalgh 2009). For thermoplastic specimens, the fracture energy is mainly absorbed by fibrillation (Fig. 10.c.K), void-coalescence (Fig. 10.c.J) and elevated plastic deformation in the resin-rich region (Fig. 10.a.D) (Greenhalgh, 2009).

At high crack speeds, fracture surface exhibits change of matrix fracture plane (Fig. 10.d.L) and radiating crystallite patterns (Fig. 10.d.M) on fiber surface (Greenhalgh, 2009). The area represented by radial features characterizes the semi crystalline structure of polyarlyetherketone (PAEK) resin system (Stumpff, 2001). Quick fracture of the polymer chains causes the pattern of these globules, developed distinctly under Mode I loading. The size and structure of these are evidence of cooling conditions during manufacturing. It has been suggested that a higher consolidating temperature results in a stronger interface explained by greater matrix deformation evidences (Greenhalgh, 2009). Crystallite patterns uniformly distributed arise where the stress mode is pure transverse tension and the fracture surface is not dominated by the formation of riverlines, scarps and cusps (Purslow, 1987).

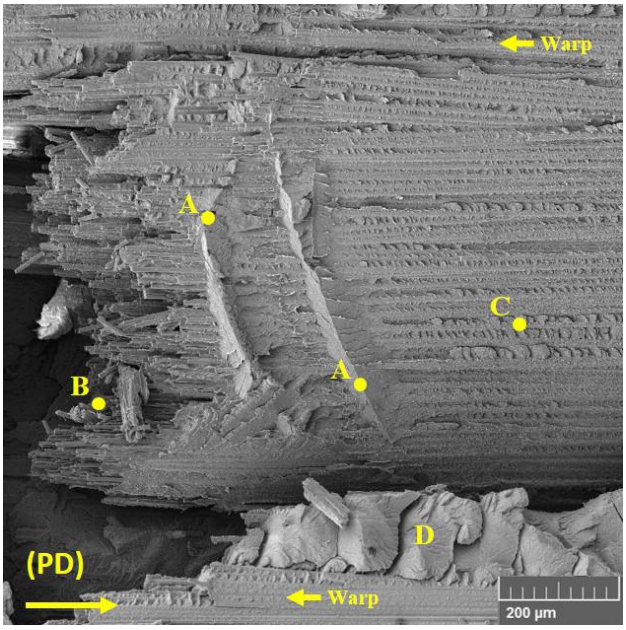

(a) Resin-rich region between two warps (x200)

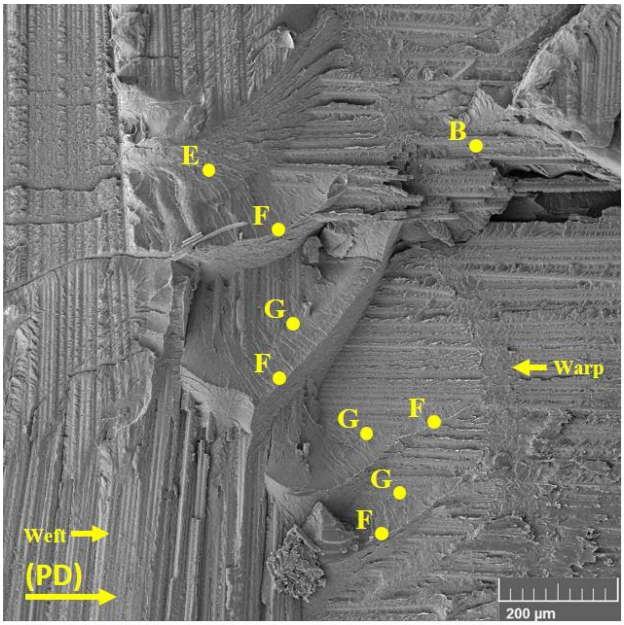

(b) Interstitial site between warp/weft tows. (x200)

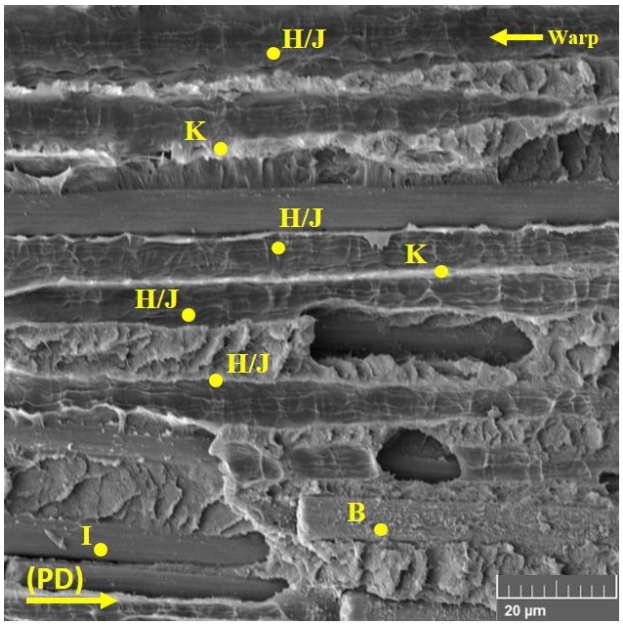

(c) Details of fiber tracks (x2000)

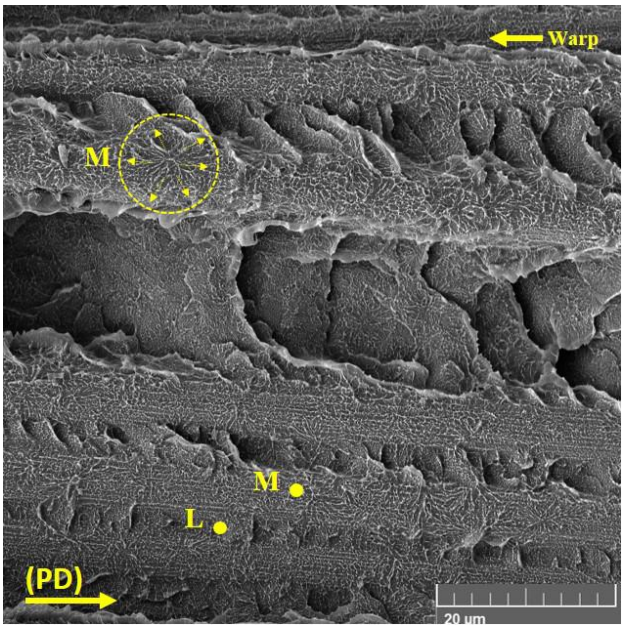

(d) Details of interface fiber/matrix. (x3000)

Figure 10. Fractography aspects

7. CONCLUSIONS

Mode I interlaminar fracture toughness in low-melt paek thermoplastic composite material was experimentally characterized using the Double Cantilever Beam (DCB) test method and experimental results in terms of load-displacement were compared with analytical predictions. The results showed satisfactory correlation between the Beam Theoretical Method and Modified Beam Theory (MBT) Method, reinforcing the idea that these methods are reliable for thermoplastic composite material.

As predicted, specimens with a thermoplastic resin system exhibit a higher fracture toughness compared to thermoset ones, in line with material available in bibliography and previous work from others researchers. Furthermore, experimental results showed unstable crack propagation.

Moreover, fractography analysis show features characteristic of Mode I failure and a Mixed-Mode behavior due to 2D nature of the fabric investigated herein. The fracture surfaces present a considerably amount of fast brittle features as scarps, cusps and riverlines. Besides, at slow crack speed, high ductility and the presence of elevated plastic deformation are noticeable.

In summary, the thermoplastic resin system proved to be interesting choice, from the interlaminar fracture toughness point of view, for application where strong consolidated joints are needed. The laminates studied in this research presented elevated fracture toughness values and high quality since fractography analysis showed a very good fiber-matrix interface with the absence of voids dispersed in the matrix.

8. ACKNOWLEDGEMENTS

The authors acknowledge the financial support received for this work from Coordenação de Aperfeiçoamento de Pessoal de Nível Superior, CAPES (Process No 88882.180816/2018-01) and Laboratory of Plasmas and Processes (LPP), Instituto Tecnológico de Aeronáutica-ITA, for allowing access to the scanning electron microscope (SEM).

9. REFERENCES

American Society for Testing and Materials, 2013. "Standard Test Method for Mode I Interlaminar Fracture Toughness of Unidirectional Fiber-Reinforced Polymer Matrix Composites". ASTM D5528

Greenhalgh, Emilie S., 2009. "Failure analysis and fractography of polymer composites". Woodhead Publishing Limited, Cambridge.

Hine, P. J., B. Brew, R. A. Duckett, and I. M. Ward, 1989. "Failure mechanisms in continuous carbon-fibre reinforced PEEK composites". Composites Science and Technology, Vol.35, pp .31-51.

Kinloch, A. J., Y. Wang, J. G. Williams, and P. Yayla., 1993. "The mixed-mode delamination of fibre composite materials". Composites Science and Technology, Vol. 47, pp. 225-237.

Murri, Gretchen B., 2013. "Evaluation of Delamination Onset and Growth Characterization Methods under Mode I Fatigue Loading". NASA Center for Aerospace Information TM–2013-217966.

Muzzy, John D., and 0. Ancil Kays, 1984. "Thermoplastic vs. Thermosetting Structural Composites". Polymer Composites, Vol.5, pp. 169-172.

O'Brien, T. Kevin., 1998. "Interlaminar fracture toughness: the long and winding road to standardization". Composites Part B, Vol. 29, pp. 57-62.

Ogasawara, T., A. Yoshimura, T. Ishikawa, R. TakahashI, N. Sasakib, and T. Ogawa., 2012. "Interlaminar fracture toughness of 5 harness satin woven fabric carbon fiber/epoxy composites". Advanced Composite Materials, Vol. 21, pp. 45-56.

Pagano, N. J., 1989. "Interlaminar Response of Composite Materials" . Elsevier Science Publishers B.V.,Wright-Patterson Air Force Base, Vol. 5.

Purslow, D., 1987. "Matrix fractography of fibre-reinforced thermoplastics, Part 1. Peel failures". Composites, Vol. 18, pp. 365-374.

Reeder, J., 2013. "Refinements to the Mixed-Mode Bending Test for Delamination Toughness". Journal of Composites, Technology and Research, Vol. 25, pp. 1-5.

Sacchetti, Francisco, J.B. Grouve, Wouter, Warnet, L.L, and Villegas, Irene., 2017 "Interlaminar fracture toughness of 5HS C/PEEK laminates. A comparison between DCB, ELS and mandrel peel tests". Polymer Testing, Vol. 66, pp. 01-28.

Stumpff, Patricia L. , 2001. "Fractography." ASM Handbook, Vol. 12, pp. 977-987.

Toyoda, Diogo Jundi., 2009. "Caracterização da tenacidade à fratura interlaminar de um material compósito de fibra de carbono-epoxi". MSc thesis, Aeronautics Institute of Technology, São José dos Campos, Brazil.

US Army Research Laboratory., 1999. "Polymer Matrix Composites: Guidelines for Characterization of Structural Materials". Composite Materials Handbook, Vol. 1.

Williams, J. G. , 1989."The Fracture Mechanics of Delamination Tests". *Journal of Strain Analysis* , Vol. 24, pp. 207-214.

10. RESPONSIBILITY NOTICE

The authors are the only responsible for the printed material included in this paper.